Article

Engineered jumpers overcome biological limits via work multiplication

https://doi.org/10.1038/s41586-022-04606-3

Received: 14 December 2020

Accepted: 3 March 2022

Published online: 27 April 2022

Check for updates

Elliot W. Hawkes[1]✉, Charles Xiao[1], Richard-Alexandre Peloquin[2], Christopher Keeley[1], Matthew R. Begley[1], Morgan T. Pope[2] & Günter Niemeyer[3]

For centuries, scientists have explored the limits of biological jump height[1,2], and for decades, engineers have designed jumping machines[3–18] that often mimicked or took inspiration from biological jumpers. Despite these efforts, general analyses are missing that compare the energetics of biological and engineered jumpers across scale. Here we show how biological and engineered jumpers have key differences in their jump energetics. The jump height of a biological jumper is limited by the work its linear motor (muscle) can produce in a single stroke. By contrast, the jump height of an engineered device can be far greater because its ratcheted or rotary motor can 'multiply work' during repeated strokes or rotations. As a consequence of these differences in energy production, biological and engineered jumpers should have divergent designs for maximizing jump height. Following these insights, we created a device that can jump over 30 metres high, to our knowledge far higher than previous engineered jumpers and over an order of magnitude higher than the best biological jumpers. Our work advances the understanding of jumping, shows a new level of performance, and underscores the importance of considering the differences between engineered and biological systems.

"Jumping [is] a peculiarly attractive subject for investigations", noted preeminent biomechanist R. M. Alexander[19]. Jumping is found across diverse species and size scales, yet is performed in strikingly similar manners and has clear, quantifiable metrics by which ultimate capabilities can be compared: jump height and distance. Indeed, the seemingly simple act of jumping has intrigued thinkers for centuries. Aristotle pondered how humans could increase jump height with halteres[1], whereas a Renaissance model approximates that all animals, regardless of size, jump roughly the same height of one metre[2]. More recent biological jumper models have examined performance limits across scale in more detail[20], incorporating effects of leg length[19], jumper height[21,22] and muscle dynamics[23–25], as well as considering the use of springs[26,27] and latches[28,29] for power-limited jumpers, and air drag for small and light jumpers[11,30]. The performance limits of jumping across scale are thus well studied within the domain of biology.

These studies have informed the design of many bio-inspired engineered jumpers, dating back to at least 1967[3]. However, a general modelling framework to capture and quantify inherent differences in biological and engineered jumpers across scale is missing from the literature. Most engineering works focus on specific designs[3–18,31], draw conclusions based on previous biological models[10], or present models that only describe single-stroke linear motors, as found in biological jumpers[14,32].

Model

Here we present a model of jumping that compares the energetics of both biological and engineered jumpers. We define a jump as a movement created by forces applied to the ground by the jumper, while maintaining a constant mass (Fig. 1a). Thus, a rocket does not jump, nor does an arrow shot from a bow. We examine two aspects of a jump: specific-energy production limits (the maximal energy that could be created for a single jump per unit mass of a jumper) and specific-energy utilization (the efficiency of converting this specific energy into jump height). We concentrate the following discussion on specific-energy production limits, as in previous biological studies[26], because we are interested in the upper bounds of jumping without any losses, and specific energy directly corresponds to the ultimate limit of jump height in a given gravitational field ($e = gh$, where g is the acceleration due to gravity and h is the jump height). (See Methods section 'Model of energy utilization' for a discussion of energy utilization non-idealities such as non-vertical motions[19], distributed mass in the spring[32] and air drag[30]).

For our analysis, we consider the following components of a jumper: a motor, an optional spring, a linkage and a payload (Fig. 1b). For the motor, we consider two types: biological and engineered (we focus on electromagnetic, though others could be substituted). Both motor types can have one of two transmission types—direct-drive (no spring) or spring-actuated (with spring)—resulting in four jumper configurations. For direct-drive transmissions, the motor directly connects via a stiff, light tendon to a linkage, the structure necessary to transmit forces to the ground. For spring-actuated (also termed power-amplified) transmissions[32–34], the motor may slowly pre-stretch a spring before the spring rapidly releases the energy into the linkage[28]; this can be done without a latch[14,29], but here we focus on the latched case. Finally, the

[1]Department of Mechanical Engineering, University of California, Santa Barbara, Santa Barbara, CA, USA. [2]Disney Research, Pasadena, CA, USA. [3]Department of Mechanical and Civil Engineering, California Institute of Technology, Pasadena, CA, USA. ✉e-mail: ewhawkes@ucsb.edu

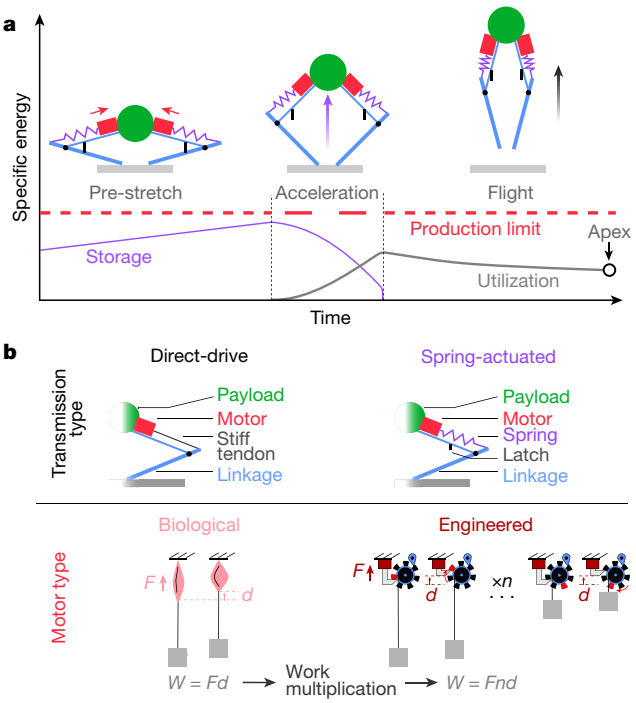

Fig. 1 | Graphical overview of the modelling framework. a, Temporally, we consider a jump to include an optional pre-stretch phase (for jumpers with latched springs), an acceleration phase during which a force is applied to the ground to accelerate the jumper upward, and a flight phase (see Supplementary Information for details of the simulation shown). Energetically, we consider two aspects of a jump. First is the specific-energy production limit (red dashed), which gives the upper bound on the energy per unit mass that can be produced. Second is the specific-energy utilization (grey curve), which terminates at the jump apex and considers losses, for example due to non-idealities in energy transfers and air drag (see Methods section 'Model of energy utilization'). Note that only the latched-spring case is shown. **b**, We categorize jumpers according to transmission type (direct-drive versus spring-actuated) and motor type (biological versus engineered). For direct-drive transmissions, the motor connects directly to the linkage, and for spring-actuated transmissions, the motor stretches a spring, which drives the jump. For biological motors (muscles), the output work W is the integral of force F over the single stroke distance d. For engineered motors, the output work is this single-stroke work multiplied by the number of strokes n; we term this increase in energy production 'work multiplication. Here a ratcheted linear motor is shown; rotary motors perform similarly (Extended Data Fig. 1).

payload comprises all remaining parts of a jumper, including the energy supply (assumed to be sufficient for multiple jumps) and non-energetic items, and we assume the payload does not directly limit or affect the single-jump energy production. We thus consider payload in Methods section 'Model of energy utilization'.

Of the energy-production components, we find the motor to have the most important differences between biological and engineered jumpers. A biological motor is a linear muscle with a finite single stroke bounding its work capacity. An engineered motor, by contrast, can overcome this single-stroke work limit. A linear engineered motor may use ratchets to combine multiple strokes (for example, in jumping microrobots)[35–38], and a rotary motor may turn repeatedly to combine multiple rotations (for example, in centimetre-scale robots)[13,15]. We term this 'work multiplication'. The number of strokes or rotations can be raised by increasing the gear reduction between the motor stroke and the jumper's overall motion (see Extended Data Fig. 1). For a direct-drive transmission, work multiplication occurs during the acceleration phase, and for a spring-actuated transmission, it primarily occurs during the pre-stretch phase. Work multiplication is available only to engineered jumpers as ratchets and rotary motors have not been found above the cellular scale in biology[39].

To describe the upper limits of specific-energy production, the model considers three primary limiters. The first limiter is the motor's single-stroke specific work[27], or the integral of specific force over stroke length (termed 'motor work limiter'). This limiter is not present for engineered jumpers, owing to work multiplication. The second limiter is the motor's specific power-time, or the product of specific power and available acceleration time[26] (termed 'motor power limiter'). The third limiter is the spring specific energy, or energy that can be stored and released per unit mass of the spring, and it is only present for spring-actuated transmissions (termed 'spring energy limiter'). We assume sufficient time between jumps to fully pre-stretch the spring regardless of the motor's power as well as sufficient spring power to discharge the energy during the acceleration time. Additionally, we consider the linkage mass necessary to transfer and apply the energy. Thus, the per-unit-mass specific jumper energy will approach but never reach its bounding limiter, especially at the high specific energies of the best engineered jumpers that require substantial linkages (for scaling of linkage mass, see Methods section 'Model of energy production limits').

Model results and insights

The results of our model (Fig. 2) show that for biological jumpers, specific-energy production can never surpass the motor work limiter, yet for engineered jumpers, the upper bound can be far greater. Specifically, biological direct-drive jumpers at a large scale (for example, a dog) can produce specific energy approaching the motor work limiter; at a small scale (for example, a lizard), the specific energy will be lower owing to power limitations[26,27,32]. Biological spring-actuated jumpers at a small scale (for example, a flea) have sufficient power, but again the specific energy is capped by the motor work limiter; at a large scale, springs are unnecessary and actually decrease the specific energy owing to added mass and muscle-spring force–displacement characteristics[26,27,32]. These trends align with previous models in the literature and biological jump data (Extended Data Fig. 2).

For engineered jumpers, work multiplication eliminates the motor work limiter. At a small scale, spring-actuated transmissions result in higher jumps than direct-drive transmissions, with an upper bound set by the spring energy limiter and the linkage mass. Theoretically, at very large scales, direct-drive transmissions are superior, with an upper bound set by the motor power limiter and the linkage mass.

These differences in energetics lead us to find that biological and engineered jumpers should have divergent designs for maximizing specific-energy production—and thus the limit on jump height. We present three key insights into these design differences. First, for biological jumpers, the crossover scale below which spring-actuated jumpers produce more specific energy and above which direct-drive jumpers produce more specific energy is approximately 1 m (0.6 s acceleration time). By contrast, for engineered jumpers, this crossover scale is nearly two orders of magnitude larger, at approximately 100 m (3 s acceleration time). (For crossover times, see Fig. 2; for conversion to scale, see Methods section 'State-space model' and Extended Data Figs. 3, 4).

Second, engineered jumpers should use a ratio of spring mass to motor mass (termed 'spring–motor mass ratio') that is much larger than that of biological jumpers (Fig. 2e). In biological systems, the motor work is the limiting factor; therefore, to maximize specific-energy production, the spring energy capacity (that is, the product of specific energy and mass) should equal but not exceed motor work (see Methods section 'Spring–motor mass ratio'). Because spring specific energy is much larger than motor specific work, only a spring mass much smaller than the motor mass is needed. We find an optimal ratio of 0.029 for biological jumpers, in line with morphological data (0.025–0.06)[26]. By contrast, for engineered jumpers with sufficient work multiplication,

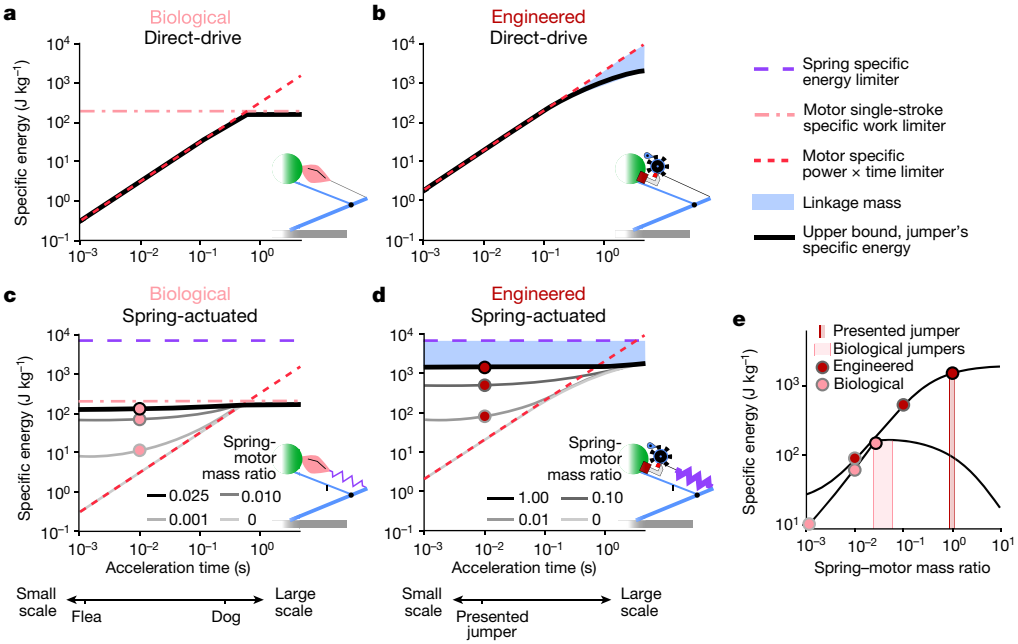

Fig. 2 | Trends of specific-energy upper bounds for biological versus engineered, and direct-drive versus spring-actuated jumpers. a–**d**, The upper bound of a jumper's specific energy (black line) will approach limiters (broken lines), but remain below owing to required linkage mass (blue shading). **a**, Biological, direct-drive: two limiters are present, (i) the motor's single-stroke specific-work limiter (the integral of the specific force over the stroke length (for muscle, approximately 200 J kg^{-1})[26], dash-dot pink), and (ii) the motor's specific power–time limiter (the product of the specific power (for muscle, approximately 200 W kg^{-1})[42] and acceleration time, dotted red). **b**, Engineered, direct-drive: because work multiplication removes the motor work limiter, only the motor power limiter is present (electromagnetic motors, approximately 2,000 W kg^{-1})[43]. **c**, Biological, spring-actuated: the addition of a latched spring helps overcome the motor power limiter, but adds a new limiter: spring specific energy (for tendon/apodeme in pure tension, approximately 7,000 J kg^{-1} (ref. [26]), dashed purple). However, the jumper's specific energy can never surpass the motor work limiter and thus never approaches the spring energy limiter. **d**, Engineered, spring-actuated: work multiplication again removes the motor work limiter, enabling the jumper's specific energy to rise toward the spring energy limiter (for latex in pure tension, approximately 7,000 J kg^{-1})[40]. **e**, These differences result in different ideal spring–motor mass ratios (the ratio of the spring mass to the motor mass) in spring-actuated jumpers: approximately 0.03 for biological and much larger for engineered. The dots in **c**–**e** mark the ratio at 0.01 s acceleration time, as measured for the presented jumper. Note that the *x* axis for **a**–**d** shows the acceleration time, to easily relate power and energy; the acceleration time relates monotonically to the length scale for an isometrically scaled jumper (see Methods section 'State-space model').

large amounts of energy can be accumulated in the spring. Thus, we find that the spring–motor mass ratio should be much larger than the ideal ratio in biological systems. Essentially, work multiplication allows engineering to better utilize the high specific energy of springs.

Third, for spring-actuated transmissions, biological jumpers should maximize the specific work of the motor, but engineered jumpers should maximize the combined specific energy of the spring plus linkage (spring-linkage specific energy). This is because each system should maximize that which primarily limits its specific energy.

From insights to jumper design

We followed these three insights to push the limits of specific-energy production, and consequently jump height, for engineered devices with electromagnetic motors. First, we chose a spring-actuated transmission, given their superiority at the selected scale of 0.3 m. Second, we set a high spring–motor mass ratio by selecting a small rotary motor (10 g) with a large gear reduction (1,000:1). This enables the motor to compress a relatively large spring with 130 N of tension in a line wrapped around its spindle (see Methods section 'Jumper design'). Third, with this peak force constraint, we designed a high-specific-energy hybrid spring-linkage via a custom nonlinear simulation framework (see Methods section 'Jumper design'). We simulated two spring-linkages that we designed based on configurations from the literature: a tension linkage[13] (passive rigid carbon fibre linkage with rubber in tension) and a compression bow[10] (bending carbon fibre without rubber; Fig. 3a). Our simulation found that the tension linkage has only slightly higher specific energy (1,638 J kg^{-1} versus 1,313 J kg^{-1}), despite the high specific energy of the rubber (7,000 J kg^{-1})[40]. To improve, we designed a hybrid tension–compression spring-linkage, supporting rubber in tension with a compression bow (1,922 J kg^{-1}). The improvement can be thought of in two ways: compared to the tension linkage, we enable the bending linkage to store energy so it is no longer passive; compared to the compression bow, we add high-specific-energy rubber in tension. Our spring-linkage also has a nearly constant force–displacement curve, which helps it store a large amount of energy given the force constraint. It provides a spring–motor mass ratio (considering the whole spring-linkage mass, 12.4 g) of 1.2 (versus 0.025–0.06 in biological jumpers)[26].

Using this hybrid spring-linkage and motor design, we created a jumper (Fig. 3b and Extended Data Fig. 5) with minimal losses in six identified stages of energy utilization (see Methods section 'Model of energy utilization'). For instance, we minimized the mass of the 'foot' (components of the jumper that are stationary during acceleration) to make energy transfer losses small, and created a shape-changing morphology that becomes streamlined after take-off to minimize air drag. We measured a payload-free specific energy of 1,075 J kg^{-1} (24.2 J per 22.5 g, see Methods section 'Jumper design'), and observed our 30-g jumper accelerating from 0 to over 28 m s^{-1} in 9 ms (>3,000 m s^{-2}) and reaching a height of 32.9 ± 0.7 m (±s.d.) (n = 3; Fig. 3c).

For comparison, we calculated a payload-free specific-energy production for the best biological jumpers of approximately 170 J kg^{-1} (ref. [26]), and for the best engineered jumpers with electromagnetic motors of approximately 100 J kg^{-1} (ref. [15]) and 115 J kg^{-1} (ref. [13]).

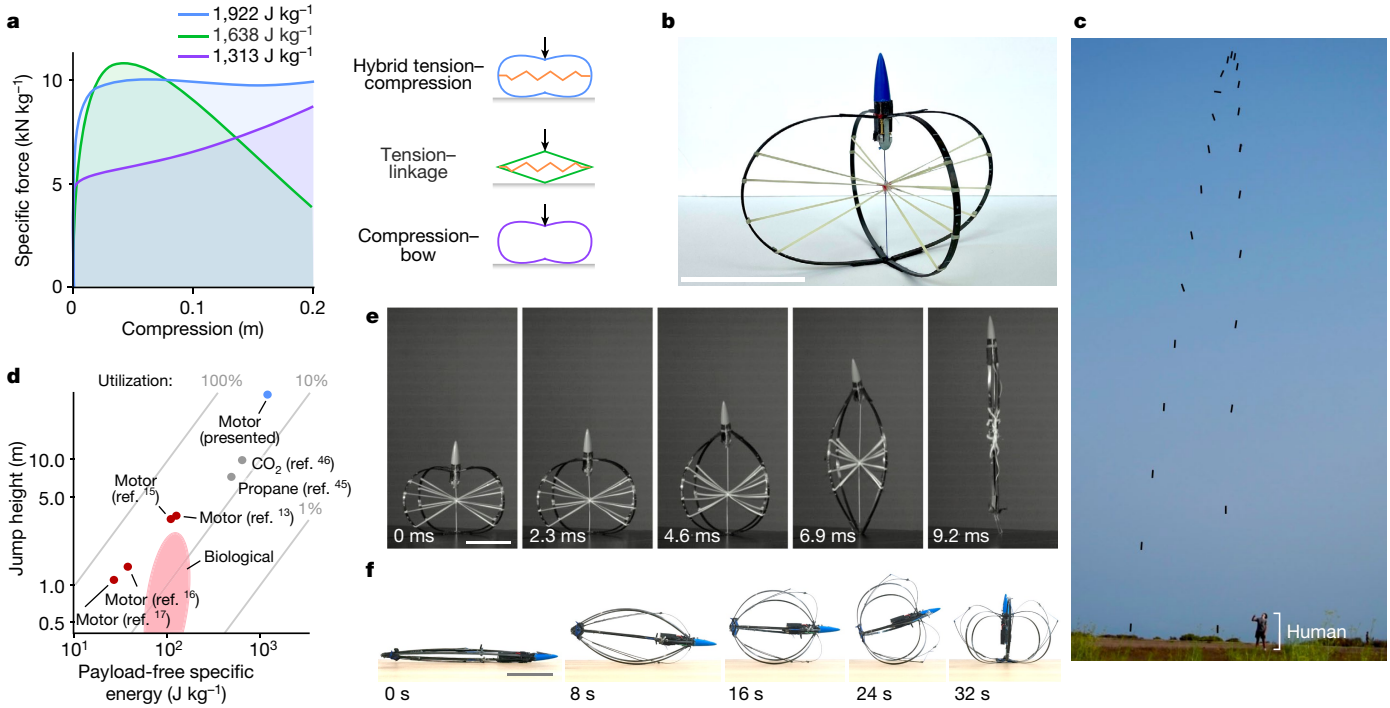

Fig. 3 | From insights to an engineered jumper that exceeds 30 m. **a**, Simulation results of the specific energy (the area under curve) for three different spring-linkage configurations: two inspired by designs from the literature (tension–linkage[13] and compression–bow[10]) and one additional design (hybrid tension–compression). **b**, The presented jumper with the hybrid spring in a stable pre-jump configuration. Scale bar, 10 cm. **c**, Image of the device jumping, with lines added over the position of the jumper every approximately 200 ms (see Supplementary Video 2). Human is 1.83 m. **d**, Jump heights of various jumpers shown as a function of payload-free specific energy. The presented jumper (blue dot) has similar utilization efficiency (grey diagonals) as previous jumpers that use electromagnetic motors (red dots), but much higher payload-free specific energy, resulting in a much higher jump. Biological jumpers tend to have lower utilization efficiency, owing to higher payloads. Two points are shown for jumpers not using electromagnetic motors, but instead propane[44] and CO_2[45]—the specific energy of propane is 10,000 kJ kg^{-1} (ref. [44]) and compressed CO_2 in a composite tank is 250 kJ kg^{-1} (ref. [46]); the payload-free specific energy is greatly reduced owing to the required structure. See Extended Data Tables 1, 2 for details of data and calculations. **e**, Frames from Supplementary Video 1 with the acceleration phase occurring in 9 ms. Scale bar, 10 cm. **f**, Frames from Supplementary Video 3 of self-righting using the legs as a roll-cage[10,17], enabled by adding four tapered legs (see Supplementary Video 4 and Methods section 'Jumper design' for details). Scale bar, 10 cm.

Considering payload and other utilization non-idealities, these specific energies result in jump heights for a galago of 2.25 m (ref. [41]) and for the engineered jumpers of 3.7 m (ref. [15]) and 3.8 m (ref. [13]).

Conclusion

In this work, we presented modelling, insights and a demonstration. Via modelling, we showed that the specific-energy production of biological jumpers cannot exceed the motor specific work, yet through work multiplication, engineered jumpers can overcome this limit, resulting in the potential to jump much higher. As a consequence, biological and engineered jumpers have different designs for maximizing specific jump energy—and the limit on jump height—which we described in three design insights. According to these, we designed a jumper that demonstrated a jump over 30 m high.

Our model suggests that this is near the feasible limit for jumpers with electromagnetic motors and currently available materials. Within specific-energy production, assuming that the spring specific energy is near the limit of available materials for solid elastic springs, the primary potential improvement is in the spring–motor mass ratio. However, even increasing the ratio from 1.2 to infinite would only increase jump height by approximately 17% (see Methods section 'State-space model' and Extended Data Fig. 6). Within specific-energy utilization, the primary improvement comes from minimizing drag effects by increasing scale; we see less room for improvement in other losses (see Methods section 'Model of energy utilization'). However, isometrically scaling the presented jumper by 10× (the predicted optimum that is large enough to eliminate drag but not too large to incur other losses) would result in only a 19% increase in jump height.

Finally, we note that our specialized design trades off adaptability, as found in biological jumpers, for high performance. Nevertheless, our results change the implications of jumping as a means of locomotion, changing how and where jumping could be used (see Supplementary Video 4). On Earth, jumping robots could overcome obstacles previously only navigated by flying robots while collecting vision-based data of the ground below (see Supplementary Video 5), and on the Moon, the leaps of the presented jumper would be even loftier: 125 m high while covering half a kilometre in a single bound. Our work fundamentally advances the understanding of the "peculiarly attractive subject"[19] of jumping and underlines the importance of considering the differences between biological and engineered systems.

Online content

Any methods, additional references, Nature Research reporting summaries, source data, extended data, supplementary information, acknowledgements, peer review information; details of author contributions and competing interests; and statements of data and code availability are available at https://doi.org/10.1038/s41586-022-04606-3.

1. Aristotle. *Problemata* 3 12–19.
2. Morowitz, H. J. De motu animalium. *Hosp. Pract.* **11**, 145–149 (1976).

3. Seifert, H. S. The lunar pogo stick. *J. Spacecr. Rockets* **4**, 941–943 (1967).
4. Zhao, J. et al. MSU jumper: a single-motor-actuated miniature steerable jumping robot. *IEEE Trans. Robot.* **29**, 602–614 (2013).
5. Niiyama, R., Nagakubo, A. & Kuniyoshi, Y. In *Proc. IEEE Intl Conf. Robotics and Automation* 2546–2551 (IEEE, 2007); https://doi.org/10.1109/ROBOT.2007.363848.
6. Scarfogliero, U., Stefanini, C. & Dario, P. In *Proc. IEEE Intl Conf. Robotics and Automation* 467–472 (IEEE, 2007); https://doi.org/10.1109/ROBOT.2007.363830.
7. Li, F. et al. Jumping like an insect: design and dynamic optimization of a jumping mini robot based on bio-mimetic inspiration. *Mechatronics* **22**, 167–176 (2012).
8. Zhao, J., Xi, N., Gao, B., Mutka, M. W. & Xiao, L. In *Proc. IEEE Intl Conf. Robotics and Automation* 4614–4619 (IEEE, 2011); https://doi.org/10.1109/ICRA.2011.5980166.
9. Churaman, W. A., Currano, L. J., Morris, C. J., Rajkowski, J. E. & Bergbreiter, S. The first launch of an autonomous thrust-driven microrobot using nanoporous energetic silicon. *J. Microelectromech. Syst.* **21**, 198–205 (2012).
10. Armour, R., Paskins, K., Bowyer, A., Vincent, J. & Megill, W. Jumping robots: a biomimetic solution to locomotion across rough terrain. *Bioinsp. Biomim.* **2**, S65–S83 (2007).
11. Bergbreiter, S. In *2008 IEEE/RSJ Intl Conf. Intelligent Robots and Systems (IROS)* 4030–4035 (IEEE, 2008); https://doi.org/10.1109/IROS.2008.4651167.
12. Koh, J. S. et al. Jumping on water: surface tension-dominated jumping of water striders and robotic insects. *Science* **349**, 517–521 (2015).
13. Woodward, M. A. & Sitti, M. MultiMo-Bat: a biologically inspired integrated jumping-gliding robot. *Int. J. Rob. Res.* **33**, 1511–1529 (2014).
14. Haldane, D. W., Plecnik, M. M., Yim, J. K. & Fearing, R. S. Robotic vertical jumping agility via series-elastic power modulation. *Sci. Robot.* **1**, eaag2048 (2016).
15. Zaitsev, V. et al. Locust-inspired miniature jumping robot. In *2015 IEEE/RSJ Intl Conf. Intelligent Robots and Systems (IROS)* 553–558 (IEEE, 2015); https://doi.org/10.1109/IROS.2015.7353426.
16. Kovač, M., Fuchs, M., Guignard, A., Zufferey, J. C. & Floreano, D. In *Proc. IEEE Intl Conf. Robotics and Automation* 373–378 (IEEE, 2008); https://doi.org/10.1109/ROBOT.2008.4543236.
17. Kovač, M., Schlegel, M., Zufferey, J. C. & Floreano, D. Steerable miniature jumping robot. *Auton. Robots* **28**, 295–306 (2010).
18. Burdick, J. & Fiorini, P. Minimalist jumping robots for celestial exploration. *Int. J. Rob. Res.* **22**, 653–674 (2003).
19. Alexander, R. M. Leg design and jumping technique for humans, other vertebrates and insects. *Phil. Trans. R. Soc. Lond. B.* **347**, 235–248 (1995).
20. Alexander, R. M. N. Simple models of human movement. *Appl. Mech. Rev.* **48**, 461–470 (1995).
21. Scholz, M. N., Bobbert, M. F. & Knoek van Soest, A. J. Scaling and jumping: gravity loses grip on small jumpers. *J. Theor. Biol.* **240**, 554–561 (2006).
22. Cerquiglini, S., Venerando, A., Wartenweiler, J. & Plagenhoef, S. Biomechanics III. In *Medicine & Science in Sports & Exercise* (ed. Hoerler, E.) vol. 6 iv (Karger AG, 1974).
23. Roberts, T. J. & Marsh, R. L. Probing the limits to muscle-powered accelerations: lessons from jumping bullfrogs. *J. Exp. Biol.* **206**, 2567–2580 (2003).
24. Bobbert, M. F. Effects of isometric scaling on vertical jumping performance. *PLoS One* **8**, e71209 (2013).
25. Azizi, E. & Roberts, T. J. Muscle performance during frog jumping: influence of elasticity on muscle operating lengths. *Proc. R. Soc. B* **277**, 1523–1530 (2010).
26. Bennet-Clark, H. C. Scale effects in jumping animals. In *Scale Effects in Animal Locomotion* (ed. Pedley, T. J.) 185–201 (Academic, 1977).
27. Sutton, G. P. et al. Why do large animals never actuate their jumps with latch-mediated springs? Because they can jump higher without them. *Integr. Comp. Biol.* **59**, 1609–1618 (2019).
28. Divi, S. et al. Latch-based control of energy output in spring actuated systems. *J. R. Soc. Interface* **17**, 20200070 (2020).
29. Longo, S. J. et al. Beyond power amplification: latch-mediated spring actuation is an emerging framework for the study of diverse elastic systems. *J. Exp. Biol.* **222**, jeb197889 (2019).
30. Bennet-Clark, H. C. & Alder, G. M. The effect of air resistance on the jumping performance of insects. *J. Exp. Biol.* **82**, 105–121 (1979).
31. Stoeter, S. A. & Papanikolopoulos, N. Kinematic motion model for jumping scout robots. *IEEE Trans. Robot.* **22**, 397–402 (2006).
32. Ilton, M. et al. The principles of cascading power limits in small, fast biological and engineered systems. *Science* **360**, eaao1082 (2018).
33. Gabriel, J. M. The effect of animal design on jumping performance. *J. Zool.* **204**, 533–539 (1984).
34. Roberts, T. J. & Azizi, E. Flexible mechanisms: the diverse roles of biological springs in vertebrate movement. *J. Exp. Biol.* **214**, 353–361 (2011).
35. Gerratt, A. P. & Bergbreiter, S. Incorporating compliant elastomers for jumping locomotion in microrobots. *Smart Mater. Struct.* **22**, 014010 (2013).
36. Greenspun, J. & Pister, K. S. J. First leaps of an electrostatic inchworm motor-driven jumping microrobot. In *2018 Solid-State Sensors, Actuators and Microsystems Workshop* 159–162 (IEEE, 2018); https://doi.org/10.31438/trf.hh2018.45.
37. Greenspun, J. & Pister, K. S. J. in *Proc. Intl Conf. Manipulation, Automation and Robotics at Small Scales (MARSS)* (eds. Haliyo, S. et al.) 258–262 (IEEE, 2017); https://doi.org/10.1109/MARSS.2017.8001944.
38. Bergbreiter, S. & Pister, K. S. J. In *Proc. IEEE Intl Conf. Robotics and Automation* 447–453 (IEEE, 2007); https://doi.org/10.1109/ROBOT.2007.363827.
39. Berg, H. C. The rotary motor of bacterial flagella. *Annu. Rev. Biochem.* **72**, 19–54 (2003).
40. Ashby, M. *Materials Selection in Mechanical Design* 4th edn (Elsevier, 2010).
41. Hall-Crags, E. C. B. An analysis of the jump of the lesser galago (*Galago senegalensis*). *J. Zool.* **147**, 20–29 (1965).
42. Josephson, R. K. Contraction dynamics and power output of skeletal muscle. *Annu. Rev. Physiol.* **55**, 527–546 (1993).
43. Seok, S., Wang, A., Otten, D. & Kim, S. In *IEEE Intl Conf. Intelligent Robots and Systems* 1970–1975 (IEEE, 2012); https://doi.org/10.1109/IROS.2012.6386252.
44. Miao, Z., Mo, J., Li, G., Ning, Y. & Li, B. Wheeled hopping robot with combustion-powered actuator. *Int. J. Adv. Robot. Syst*. https://doi.org/10.1177/1729881417745608 (2018).
45. Ackerman, E. Boston dynamics sand flea robot demonstrates astonishing jumping skills. *IEEE Spectrum Robotics Blog* https://spectrum.ieee.org/boston-dynamics-sand-flea-demonstrates-astonishing-jumping-skills (28 March 2012).
46. Dowling, K. *Power Sources for Small Robots*. Technical report no. CMU-RI-TR-97-02 (Carnegie Mellon University, 1997).

Methods

Model of energy production limits

We first consider the maximum energy that could be available to the jumper, dependent on its components. We consider the payload, which we assume does not directly limit or affect the single-jump energy production in the energy utilization model, and segment the remainder of the jumper as follows: (i) a motor, providing the mechanical energy, (ii) optional elastic energy storage or springs, temporarily accumulating mechanical energy, and (iii) inelastic linkage or other elements, applying the energy via ground reaction forces. In the extremes, the jumper may contain no springs (purely inelastic), or it may use the springs for structural support and require little to no inelastic linkage elements. Note that we include linkage mass in the energy production instead of utilization, as neither motors nor springs can operate in isolation. Indeed, to fairly evaluate the energy production, we must consider how much linkage mass a design requires to function. We begin with direct-drive transmissions before considering spring actuation. Also note that specific energy per unit mass is denoted by a lowercase e, compared to absolute energy, which is denoted by an uppercase E.

Direct-drive transmission. We determine the maximum specific jump energy, $e_{\text{jump}}^{\text{direct}}$, assuming the jumper contains only a motor of mass m_{m} and a linkage of mass m_{l}. In biological systems, the muscle's specific energy is limited by the maximum specific work of a full stroke:

$$e_{\text{m}}^{\text{bio}} = \frac{1}{m_{\text{m}}}\int_0^d F(x)_{\max}\,\mathrm{d}x,$$

defined by integrating the maximum force, $F(x)_{max}$, over the entire stroke, d. In engineering, a linear motor with the addition of a ratchet could complete multiple strokes to overcome such a limit. Similarly, a rotary motor has an unlimited stroke and hence an unlimited energy (limited ultimately only by the energy supply; because battery specific energy is orders of magnitude larger than those considered in this analysis, approximately 500 kJ kg^{-1} (ref. [46]), we assume it is nearly infinite). We generally apply

$$e_{\text{m}}^{\text{eng}} = \infty.$$

Interestingly, biological muscle ratchets at a microscopic scale, but its macroscopic structure loses the feature and limits its stroke.

Both biological and engineered motors are also limited by their maximum specific power $p_{\text{m}} = P_{\text{m}}/m_{\text{m}}$, available during the acceleration time, t_0. The specific jump energy is thus limited by both as

$$e_{\text{jump}}^{\text{direct}} = \frac{E_{\text{jump}}^{\text{direct}}}{m_{\text{m}}+m_{\text{l}}} = \frac{\min(E_{\text{m}},\, P_{\text{m}}t_0)}{m_{\text{m}}+m_{\text{l}}}$$
$$= \frac{\min(m_{\text{m}}e_{\text{m}},\, m_{\text{m}}p_{\text{m}}t_0)}{m_{\text{m}}+m_{\text{l}}} = m_{\text{m}}\frac{\min(e_{\text{m}},\, p_{\text{m}}t_0)}{m_{\text{m}}+m_{\text{l}}}.$$

Spring-actuated transmission. We further include a spring of mass m_{s}, with a maximum specific-energy capacity of $e_{\text{s}} = E_{\text{s}}/m_{\text{s}}$. If we allow the motor a pre-stretch time t_{p}, the spring may store energy up to

$$E_{\text{store}} = \min(m_{\text{s}}e_{\text{s}},\, m_{\text{m}}e_{\text{m}},\, m_{\text{m}}p_{\text{m}}t_{\text{p}}).$$

If we allow the motor to continue providing energy during the acceleration phase (not possible for many jumper designs, but represents the upper limit) and assume the spring can deliver specific power up to $p_{\text{s}} = P_{\text{s}}/m_{\text{s}}$, we have a maximum specific jump energy of:

$$e_{\text{jump}}^{\text{spring}} = \frac{E_{\text{jump}}^{\text{spring}}}{m_{\text{m}}+m_{\text{s}}+m_{\text{l}}} = \frac{\min(m_{\text{m}}e_{\text{m}},\, E_{\text{store}}+m_{\text{m}}p_{\text{m}}t_0,\, m_{\text{s}}p_{\text{s}}t_0)}{m_{\text{m}}+m_{\text{s}}+m_{\text{l}}}.$$

Finally, if we assume the spring's output specific power p_{s} far exceeds the requirements $p_{\text{s}} \gg e_{\text{s}}/t_0$, we find

$$e_{\text{jump}}^{\text{spring}} = \frac{E_{\text{jump}}^{\text{spring}}}{m_{\text{m}}+m_{\text{s}}+m_{\text{l}}} = \frac{\min\,(m_{\text{m}}e_{\text{m}},\, m_{\text{m}}p_{\text{m}}(t_{\text{p}}+t_0),\, m_{\text{s}}e_{\text{s}}+m_{\text{m}}p_{\text{m}}t_0)}{m_{\text{m}}+m_{\text{s}}+m_{\text{l}}}.$$

Spring–motor mass ratio. The mass ratio is used in Fig. 2. We see that increasing the spring mass m_{s} helps only when the system is neither limited by motor energy nor by motor power:

$$e_{\text{jump}}^{\text{spring}} = \frac{m_{\text{m}}}{m_{\text{m}}+m_{\text{s}}+m_{\text{l}}}\min(e_{\text{m}},\, p_{\text{m}}(t_{\text{p}}+t_0),\, \frac{m_{\text{s}}}{m_{\text{m}}}e_{\text{s}}+p_{\text{m}}t_0).$$

Thus, assuming sufficient pre-stretch time t_{p}, biological jumpers are helped up to an optimal mass ratio where $e_{\text{m}} = \frac{m_{\text{s}}}{m_{\text{m}}}e_{\text{s}} + p_{\text{m}}t_0$, or

$$\left(\frac{m_{\text{s}}}{m_{\text{m}}}\right)_{\text{optimal}} = \frac{e_{\text{m}}-p_{\text{m}}t_0}{e_{\text{s}}} \approx \frac{e_{\text{m}}}{e_{\text{s}}},$$

which equates to ~0.029 when values of e_{m} and e_{s} from Fig. 2 are used (~200 J kg^{-1} and ~7,000 J kg^{-1}, respectively). By contrast, adding spring mass to engineered jumpers helps indefinitely, approaching the maximal specific energy

$$(e_{\text{jump}}^{\text{spring}})_{\text{limit}} = \frac{m_{\text{s}}e_{\text{s}}+m_{\text{m}}p_{\text{m}}t_0}{m_{\text{m}}+m_{\text{s}}+m_{\text{l}}} \to \frac{m_{\text{s}}}{m_{\text{s}}+m_{\text{l}}}e_{\text{s}},$$

assuming that the linkage mass m_{l} also needs to increase to support the higher energies.

Size/length scaling. Beyond mass ratios, the jump energy limit depends only on the motor/spring specific energy/power properties, as well as the pre-stretch time (which we assume can be freely selected) and the acceleration time, t_0. The specific energies and powers are assumed to be scale-invariant: in biology[47,48], muscle forces scale with area, $F_{\max} \propto L^2$, whereas distance (stroke) and velocity scale with length, $d \propto L$, $v_{\max} \propto L$, and mass scales with volume, $m \propto L^3$. In engineering, with electromagnetic rotary motors, the torque scales with the 4th power of length, $\tau \propto L^4$, whereas the angular speed scales inverse linearly, $\omega \propto L^{-1}$, so again the power remains scale invariant[47,49,50]. Similar to biological muscle, all spring forces scale with area, $F_{\max} \propto L^2$, whereas distances (stroke) scale with length, $d \propto L$, such that spring specific energies are scale-independent.

We also note that assume the required linkage mass m_{l} simply scales with jump energy: to maintain a constant stress across scale, the cross-sectional area of the linkage will scale with force $F_{\max}$, whereas the length scales with stroke d. As such, we can define a scale-invariant specific-energy transfer capacity,

$$e_{\text{l}} = \frac{E_{\text{jump}}}{m_{\text{l}}}.$$

Equivalently, and again assuming sufficient pre-stretch time t_{p}, we write the required linkage mass as

$$m_{\text{l}} = \frac{E_{\text{jump}}}{e_{\text{l}}} = \frac{\min(m_{\text{m}}e_{\text{m}},\, m_{\text{s}}e_{\text{s}}+m_{\text{m}}p_{\text{m}}t_0)}{e_{\text{l}}},$$

to obtain

$$e_{\text{jump}} = \frac{E_{\text{jump}}}{m_{\text{m}} + m_{\text{s}} + m_{\text{l}}} = \frac{1}{\frac{1+\frac{m_{\text{s}}}{m_{\text{m}}}}{\min\left(e_{\text{m}}, \frac{m_{\text{s}}}{m_{\text{m}}} e_{\text{s}} + p_{\text{m}} t_0\right)} + \frac{1}{e_{\text{l}}}}.$$

For a spring-actuated engineered jumper, this brings the maximal specific energy for an infinite spring–motor mass ratio to

$$(e_{\text{jump}})_{\text{eng-limit}} = \frac{1}{\frac{1}{e_{\text{s}}} + \frac{1}{e_{\text{l}}}} = \frac{e_{\text{s}}\ e_{\text{l}}}{e_{\text{s}} + e_{\text{l}}}.$$

We note that this final expression is similar to how stiffnesses of springs add in series. In Fig. 2, we approximate for engineering e_{l} as 2,650 J kg^{-1}, based on the values from our jumper (where e_{s} = 7,000 J kg^{-1} and $(e_{\text{jump}}^{\text{spring}})$ = 1,922 Jkg^{-1}). For a motor-work-limited biological jumper with minimal spring mass, we calculate

$$(e_{\text{l}})_{\text{bio}} = \frac{e_{\text{m}} m_{\text{m}}}{m_{\text{l}}},$$

as 1,130 J kg^{-1}, based on the values for muscle specific energy (200 J kg^{-1}) and per cent of mass of the skeleton (~14%)[51].

Only the acceleration time t_0 is scale-dependent (for both direct-drive and spring-actuated transmission types). For isometric scaling assumptions, the acceleration time monotonically increases with scale. More specifically, for all but the largest direct-drive jumpers, configured to operate at peak power during the entire acceleration phase, time scales with a 2/3 power, $t_0 \propto L^{2/3}$ (see Methods section 'State-space model' below, and previous biological model[26]). Meanwhile, the acceleration time for spring-actuated jumpers increases linearly with scale, $t_0 \propto L$ (also see Methods section 'State-space model').

We finally note that our model, showing that spring-powered jumpers are scale-invariant in specific-energy production, contrasts with the conclusions of previous work[32], which stated that specific-energy production decreases at small scales for spring-powered jumpers. The discrepancy arises from differing model assumptions: the previous work, in an effort to model not just jumpers but also many other high-power movements, considered a catapult launching a projectile, where only the projectile, but not the catapult, changed size during scaling. This led to the conclusion that the catapult's spring would meet material limits; however, during scaling of a jumper, spring and all, this effect is not present, and spring-powered biological jumpers should be scale-invariant, as shown in more recent work[27].

Model of energy utilization

An energy utilization model is a helpful design tool, as it describes the effects of different losses on the achievable jump height, h, (defined as the change in vertical centre-of-mass position from standing to apex), given a maximum payload-free specific jump energy, e_{jump}. Using an energy flow perspective, we lump all losses and reductions into the following six types or stages. We note that many of the individual components have been discussed in separate papers, as referenced below, and that this general framework that assembles disparate models is helpful for design and analysis. Further, we realize the numerical computation of each reduction may require assumptions or approximations (see the Supplementary Information for derivations). The six stages, with losses given in parentheses, are:

1. Produced specific energy: $e_{\text{prod}} = e_{\text{jump}}\eta_{\text{prod}}$ (reduced by production inefficiency).
2. Available specific energy: $e_0 = e_{\text{prod}}\left[1 - \frac{m_{\text{payload}}}{m}\right]$ (adjusted for payload apportionment).
3. Specific kinetic energy (KE), total: $e_{\text{KE}} = e_0 - Lg\frac{m_{\text{body}}}{m}$ (less energy needed to stand).
4. Specific kinetic energy, vertical: $e_{\text{vert}} = e_{\text{KE}}[1 - \beta_{xy} - \beta_{\theta}]$ (less non vertical energy).
5. Specific kinetic energy, centre of mass (COM): $e_{\text{COM}} = e_{\text{vert}}\left[1 - \frac{m_{\text{foot}}}{m}\right]$ (less energy transfer losses).
6. Specific potential energy, centre of mass: $e_{\text{apex}} = e_{\text{COM}}\left[1 - \frac{D_{\text{s}} e_{\text{COM}}}{2}\right]$ (less aerodynamic drag losses).

Where η_{prod} is production efficiency, m_{payload} is the mass of the payload, m is the total mass, m_{body} is the lumped mass that is moving during acceleration (see Supplementary Information), m_{foot} is the lumped mass that is static, β_{xy} and β_{θ} are the fraction of the kinetic energy due to movements in any horizontal direction and due to rotations, respectively, and D_{s} is a drag constant (see Supplementary Information). Overall, we write the model as:

$$h = \frac{1}{g}e_{\text{apex}} = \frac{1}{g}\left[e_{\text{jump}}\eta_{\text{prod}}\left(1 - \frac{m_{\text{payload}}}{m}\right) - Lg\frac{m_{\text{body}}}{m}\right]$$
$$\left[1 - \beta_{xy} - \beta_{\theta}\right]\left[1 - \frac{m_{\text{foot}}}{m}\right]\left[1 - \frac{D_{\text{s}} e_{\text{COM}}}{2}\right].$$

Further details of each stage:

1. Produced specific energy, e_{prod}, considering the production efficiencies: Any impedance mismatches between components or viscous losses will reduce the available energy. Practically, the force–displacement profiles of biological muscle and tendons limits jumpers to obtain 30–50% of the potential muscle energy[26,27]. By contrast, our nearly constant force spring matches the nearly constant force output of our motor, mitigating this loss. Further, a very small damping ratio (0.02) was experimentally determined for the carbon fibre experimentally measured using a clamped beam oscillation method[52].

2. Initial specific energy before movement, e_0, that can be released in a single jump: Any payload requires apportionment across the entire mass[26]. Our jumper has a payload-free mass of 22.5 g and payload mass of only 7.9 g. Thus the 1,075 J kg^{-1} payload-free specific energy is reduced to 796 J kg^{-1} in this step. However, we see little room for improvement here. Our battery is a lithium polymer battery, which is the lightest commercially available option. Our release mechanism has a mass of 1.23 g (made from 7075 aluminium) and our nose cone 1.2 g. All other components are less than a gram.

3. Total specific kinetic energy, e_{KE}, after the full stroke has occurred: This deducts the potential energy surrendered to raise the centre of mass from crouch to stand[21]. This delivers the jump height as the change in height of the centre of mass above its position when the jumper is fully standing. Our jumper has negligible loss here, owing to its small size and high jump.

4. Vertical specific kinetic energy, e_{vert}, due to movements in the vertical (z) direction only[19]. This deducts the fraction of the kinetic energy due to movements in any horizontal direction (β_{xy}) and due to rotations (β_{θ}). This also includes potential losses due to sliding on the ground surface or frictional losses in joints. Along with (5), below, our jumper has roughly 50% efficiency for these stages. Interestingly, a pure compression spring of a solid material with only vertical motion mitigates this non-vertical loss, but is only 50% for the energy transfer loss. Alternatively, a realistic compression spring, such as a coil or bow spring, will have substantial non-vertical motion, meaning its efficiency will be below 50%. Our device exceeds 50% because of its payload, which is placed at the top of the jumper, whereas the 'foot' mass is minimized (only the bottom of the spring).

5. Vertical centre-of-mass specific kinetic energy, e_{COM}, after launch: This deducts the transfer losses shifting energy from individual masses to the centre-of-mass motion[18,19,32]. It effectively removes energy of internal relative motions, accelerating the foot and the portion of the spring that was stationary prior to launch.

6. Potential energy at the jump apex, e_{apex}: This deducts the aerodynamic drag losses occurring during the jump[11,30]. Our jumper loses about 25% of its energy owing to air drag, even with its highly

streamlined body. This loss is possible to mitigate by scaling 10× (Extended Data Fig. 6).

Regarding isometric scaling, we note that the energy-to-stand losses dominate at large scales. For any jumper with a scale-invariant maximum jump energy, we find a maximum standing height

$$L_{\text{stand}} = \frac{1}{g}\frac{m - m_{\text{payload}}}{m - m_{\text{foot}}}\eta_{\text{prod}} e_{\text{jump}},$$

beyond which jumping is no longer possible. Meanwhile, at small scales the aerodynamic losses dominate. See Methods section 'State-space model' and Supplementary Information section 'Energy utilization model' for further details.

State-space model: adding jumper specifics

We also simulate jumpers using a simple second-order model. Assume a single moving lumped body mass, m_b, with vertical position z, velocity v, acceleration a, consistent with previous jumping models[32]. The jumper has a length scale, L, which we define as the leg stroke, or difference between the body height when the jumper is fully crouched ($z = 0$) and when standing ($z = L$); the jump height is measured above $z = L$. This model neglects the effects of geometric linkages, motor internal inertias, multiple masses, and so on, but captures the fundamental power and energy production and predicts acceleration times relative to the jumper scale. We consider direct-drive and spring-actuated transmissions.

Direct-drive transmission. Assume the body is driven, via a reduction G, by an inertia-free motor with linear viscous losses:

$$m_b a = GF_m\left(1 - \frac{Gv}{v_m}\right) - m_b g,$$

where F_m and v_m are the motor's maximum force and velocity, respectively. We consider both fixed reductions and variable reductions, where the motor continually operates at maximum power. The latter case is modelled by

$$m_b a = \frac{F_m v_m}{4v} - m_b g = \frac{m_m p_m}{v} - m_b g.$$

We again note that biological and engineered motor specific power is scale-invariant[47,49,50]:

$$p_m = \frac{F_m v_m}{4m_m} = \text{constant}.$$

For biological jumpers, assume G is upper-bound by a value of one, in the case when the muscle completes a full stroke during the leg stroke. Consequently, the scale-invariant motor specific energy is

$$e_m^{\text{bio}} = \frac{F_m L}{m_m} = \text{constant}.$$

We simulate a payload-free system using the same motor parameters as described in Fig. 2. The body mass is composed of the motor and linkage mass such that $m_b = m_s + m_l$. Extended Data Fig. 3 graphs the results.

Not surprisingly, operating at maximum power, when possible, delivers the most energy. It also provides acceleration times scaled with a 2/3 power of size. We further note that the biological jumper's finite motor stroke limits both the maximum power operation and the "reduction. As such, large-scale animals have limited energy and see a drop off in their kinetic energy owing to increasing energy to stand, ultimately limiting the size of animals that can jump. By contrast, linkage-less engineered jumpers theoretically can produce more energy the larger they are (Extended Data Fig. 3a), with kinetic energy plateauing with scale (Extended Data Fig. 3b); when linkage mass is considered, produced energy instead plateaus (Extended Data Fig. 3a) and kinetic energy drops off (Extended Data Fig. 3b).

Spring-actuated transmission. Alternatively, assume that the motor pre-stretches a latched linear spring-linkage assembly of additional mass m_s. In turn, when fully stretched and released, the spring propels the body upward. If the spring shows uniformly distributed mass and uniform strain rate, then effectively $\frac{1}{2}m_s$ contributes to potential energy, and $\frac{1}{3}m_s$ contributes to kinetic energy. We can thus model

$$\left(m_b + \frac{1}{3}m_s\right)a = k(L - z) - \left(m_b + \frac{1}{2}m_s\right)g,$$

where the stiffness, k, relates to the effective spring specific energy:

$$e_s = \frac{\frac{1}{2}kL^2}{m_s}.$$

This implicitly maps the appropriate portion of the spring to the foot and body. We again simulate the system using the spring specific energy from Fig. 2 and assume the body mass consists of only a motor mass. We then vary the effective spring–motor mass ratio.

Extended Data Fig. 4 shows the results. We note that, for such spring-actuated jumpers, the acceleration time increases linearly with scale. We also see that smaller springs impose a limit on the size of jumper—smaller spring forces cannot overcome larger weights. And naturally, smaller springs provide less energy, specific to the total jumper mass.

A more detailed description of state space model is found in Supplementary Information.

Jumper design

Spring material selection. We search a material database to maximize the 'material factor', or the ratio of the elastic stored energy during axial extension to mass:

$$\kappa = \frac{\sigma_y^2}{E\rho},$$

where σ_y is the yield stress, E is the modulus of elasticity, and ρ is the density (Extended Data Fig. 5a). The largest material factor occurs among two main groups of materials: elastomers at lower values of E/ρ (we choose latex rubber), and fibre-reinforced composites at higher values of E/ρ (we choose carbon-fibre composite). See Supplementary Information for further details.

Spring design. To explore the design space of springs, we built a nonlinear quasistatic simulation framework, comparing the three designs outlined in the main text. The simulation provides a guideline for selecting spring parameters for designing a hybrid spring, suggesting ratios of rubber cross-section to length for a given carbon fibre cross-section to length, such that peak strain in the carbon fibre is reduced compared to the no-rubber case. See Supplementary Information for details of the simulation and comparison.

Jumper design. A small highly geared motor reels in an ultrahigh-molecular-weight polyethylene line (Spectra) to compress the spring, storing ~24.2 J of energy at >90% of the bow ultimate strength. A lightweight release mechanism unlatches to relieve the tension in the line and initiate a jump (see Extended Data Fig. 5). We mount the motor, this release mechanism, the batteries and the nose cone at the top of the bows. Placing as much of the necessary mass on the moving body helps reduce the foot mass ratio and improves the energy transfer in stage 4 of the energy utilization model.

We power the motor using a small lithium polymer cell battery (enough energy for roughly ten jumps). The battery is packaged in a model rocket nose cone that helps reduce the drag of the jumper. To further reduce drag, the robot shape-changes during the acceleration phase, from a wide, stable configuration to a streamlined, rocket-like shape (see Supplementary Videos 6, 7). Cyanoacrylate adhesive is used throughout for bonding. The combination of a lightweight construction and high-strength materials means the jumper can survive landing on even concrete surfaces from its apex height of over 30 m. All of the components are shown in Extended Data Fig. 5d and listed in Extended Data Table 3.

Release mechanism. The goals of the release mechanism are to quickly release tension in the string that compresses the bow spring (extension of the spring occurs in less than 9 ms), enable resetting for another jump, manage the high forces (~130 N), and be as light as possible. This is achieved with a hinged arm that supports a roller, which turns on bearings, and over which the string passes (Extended Data Fig. 5c). A latch opens to release the tension from the string, after which a rubber band resets the arm, allowing the motor to begin winding for another jump without ever stopping. Given the small size of the motor, reset time is roughly 2 min. This could be decreased by increasing the motor size (for example, doubling the motor mass (and power) would approximately halve the reset time).

Self-righting mechanism. To right between jumps, a simple modification to the jumper can be made: adding four bows, one between each set of the main bows, that are tapered and split such that they have an asymmetric shape when compressed (Extended Data Fig. 5e and Fig. 3f). The concept of a roll cage has been employed previously for self-righting[10,17]. In the presented design, the tapered and split bows contact the ground and deform during compression to push the jumper upright (see Supplementary Video 3).

Determining the payload-free specific energy of the jumper. This value can be determined as the energy the motor is able to store in the spring-linkage per mass of the motor and spring-linkage. A force–displacement curve was measured for the hybrid compression–tension spring, using the displacement that the motor is able to create (20.3 cm; Extended Data Fig. 5b). The stored energy is measured as 24.2 J, the hybrid spring-linkage mass as 12.4 g, and motor mass as 10.1 g; thus, we find an overall payload-free specific energy of 1,075 J kg^{-1}.

Data availability

All data are available in Extended Data Tables 1–3.

Code availability

MATLAB code for the energy production and utilization models and the state-space model, as well as the spring simulation, are available upon request.

47. Marden, J. H. & Allen, L. R. Molecules, muscles, and machines: universal performance characteristics of motors. *Proc. Natl. Acad. Sci. USA* **99**, 4161–4166 (2002).
48. Hirt, M. R., Jetz, W., Rall, B. C. & Brose, U. A general scaling law reveals why the largest animals are not the fastest. *Nat. Ecol. Evol.* **1**, 1116–1122 (2017).
49. Winslow, J., Hrishikeshavan, V. & Chopra, I. Design methodology for small-scale unmanned quadrotors. *J. Aircr.* **55**, 1062–1070 (2018).
50. Dermitzakis, K., Carbajal, J. P. & Marden, J. H. Scaling laws in robotics. *Procedia Comp. Sci.* **7**, 250–252 (2011).
51. Mitchell, H. H., Hamilton, T. S., Steggerda, F. R. & Bean, H. W. The chemical composition of the adult human body and its bearing on the biochemistry of growth. *J. Biol. Chem.* **158**, 625–637 (1945).
52. Hunt, J. F., Zhang, H., Guo, Z. & Fu, F. Cantilever beam static and dynamic response comparison with mid-point bending for thin mdf composite panels. *BioResources* **8**, 115–129 (2013).
53. Parry, D. A. & Brown, R. H. J. The jumping mechanism of salticid spiders. *J. Exp. Biol.* **36**, 654–664 (1959).
54. Marsh, R. L. & John-Alder, H. B. Jumping performance of hylid frogs measured with high-speed cine film. *J. Exp. Biol.* **188**, 131–141 (1994).
55. Evans, M. E. G. The jump of the click beetle (Coleoptera, Elateridae)—a preliminary study. *J. Zool.* **167**, 319–336 (1972).
56. Brackenbury, J. & Hunt, H. Jumping in springtails: mechanism and dynamics. *J. Zool.* **229**, 217–236 (1993).
57. Maitland, D. P. Locomotion by jumping in the Mediterranean fruit-fly larva *Ceratitis capitata*. *Nature* **355**, 159–161 (1992).
58. Harty, T. H. *The Role of the Vertebral Column during Jumping in Quadrupedal Mammals*. PhD thesis, Oregon State Univ. (2010).
59. Schwaner, M. J., Lin, D. C. & McGowan, C. P. Jumping mechanics of desert kangaroo rats. *J. Exp. Biol.* **221**, jeb186700 (2018).
60. Katz, S. L. & Gosline, J. M. Ontogenetic scaling of jump performance in the african desert locust (*Schistocerca gregaria*). *J. Exp. Biol.* **177**, 81–111 (1993).
61. Toro, E., Herrel, A., Vanhooydonck, B. & Irschick, D. J. A biomechanical analysis of intra- and interspecific scaling of jumping and morphology in Caribbean *Anolis* lizards. *J. Exp. Biol.* **206**, 2641–2652 (2003).
62. Essner, R. L. Three-dimensional launch kinematics in leaping, parachuting and gliding squirrels. *J. Exp. Biol.* **205**, 2469–2477 (2002).
63. Gregersen, C. S. & Carrier, D. R. Gear ratios at the limb joints of jumping dogs. *J. Biomech.* **37**, 1011–1018 (2004).
64. Burrows, M. & Dorosenko, M. Jumping mechanisms and strategies in moths (Lepidoptera). *J. Exp. Biol.* **218**, 1655–1666 (2015).
65. Bobbert, M. F., Gerritsen, K. G. M., Litjens, M. C. A. & Van Soest, A. J. Why is countermovement jump height greater than squat jump height? *Med. Sci. Sports Exerc.* **28**, 1402–1412 (1996).
66. Brackenbury, J. & Wang, R. Ballistics and visual targeting in flea-beetles (Alticinae). *J. Exp. Biol.* **198**, 1931–1942 (1995).
67. Burrows, M. Jumping performance of froghopper insects. *J. Exp. Biol.* **209**, 4607–4621 (2006).

Acknowledgements We thank W. Heap for assistance with jumper design and testing, K. Chen for assistance testing jumpers, F. Porter for assistance with modelling, H. Bluestone for editorial suggestions, G. Hawkes for early discussions on the limits of jumping, S. Rufeisen and K. Park for help filming, A. Sauret for sharing high-speed videography equipment, and K. Fields for technical support. This work was partially supported by an Early Career Faculty grant from NASA's Space Technology Research Grants Program.

Author contributions E.W.H., M.T.P. and G.N. designed the research; E.W.H., R.-A.P. and C.K. performed the experiments; E.W.H., M.T.P., G.N., C.K., C.X. and R.-A.P. analysed the data; C.X., M.R.B. and G.N. performed modelling and simulations; C.K., R.-A.P. and E.W.H. built the jumpers; E.W.H., G.N. and C.X. wrote the paper; E.W.H., M.T.P. and G.N. supervised the project.

Competing interests The authors declare no competing interests.

Additional information
Supplementary information The online version contains supplementary material available at https://doi.org/10.1038/s41586-022-04606-3.

Correspondence and requests for materials should be addressed to Elliot W. Hawkes.

Peer review information *Nature* thanks Sawyer Fuller, Gregory Sutton and the other, anonymous, reviewer(s) for their contribution to the peer review of this work. Peer reviewer reports are available.

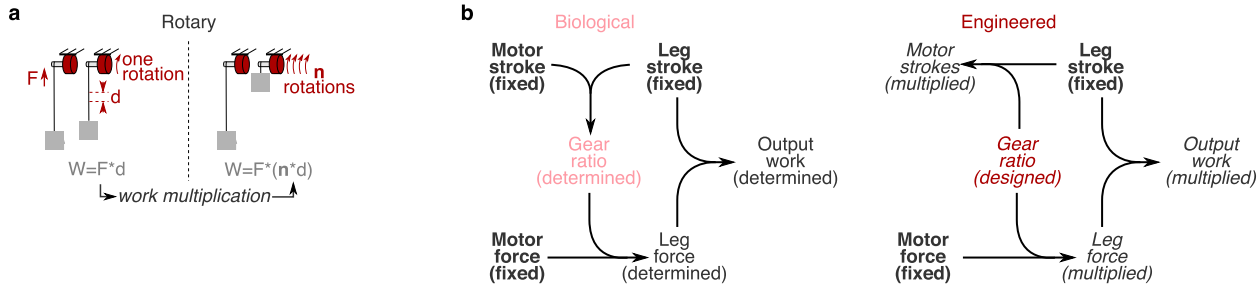

Extended Data Fig. 1 | Work multiplication in more detail. a, Similar to a ratcheted motor in Fig. 1, a rotary motor can accomplish work multiplication through multiple rotations instead of multiple strokes. **b**, The output work of a biological jumper is determined by fixed parameters (motor stroke, leg stroke and motor force), but work multiplication overcomes this for engineered jumpers: For biological jumpers, motor stroke and leg stroke determine an effective gear ratio, if the entire stroke of both is to be used (in animals, the gear ratio varies around this value slightly throughout the jump)[19]. With this determined gear ratio and a fixed motor force (assuming a size of motor), the leg force is determined. Finally, with the fixed leg stroke and determined leg force, the output work is determined. By contrast, for engineered jumpers, although the leg stroke is roughly fixed (assuming a size of jumper), the motor can make multiple strokes or rotations, allowing the gear ratio to be designed (higher gear ratio will result in more strokes, at the cost of more time). With this designed gear ratio and a fixed motor force (assuming a size of motor), the leg force is also multiplied with respect to the leg force in the single-stroke case. Finally, with the fixed leg stroke and the multiplied leg force, the output work is also multiplied.

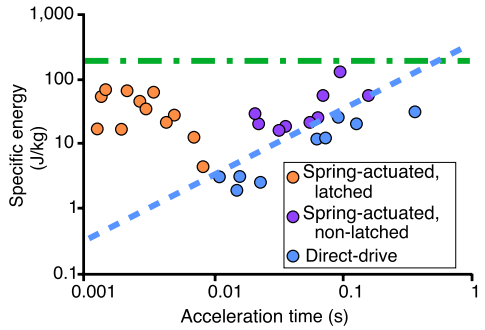

Extended Data Fig. 2 | Biological mechanism specific-energy data. The model (Fig. 2a–c) predicts an upper limit to specific energy for all biological jumping mechanisms, regardless of transmission type, at approximately 200 J kg^{-1} (dash-dot green). Across scales found in nature, this limit holds. Note that the energy utilization was estimated at 15%, similar to previous biological work[26,27]. However, variation likely occurs, with jumpers with higher take-off velocities likely having more mass dedicated to jumping muscles, and thus having a higher energy utilization efficiency. A higher utilization efficiency, for example, 30%, would result in a lower mechanism specific energy than shown here. The model also predicts a limit due to motor specific power. Direct-drive jumpers fall on or below this limit (dashed blue). Non-latched spring-actuated jumpers can exceed this limit, and latched spring-actuated jumpers can exceed it by even greater amounts (distance from blue dashed line). However, all still fall below. See Extended Data Table 1 for data.

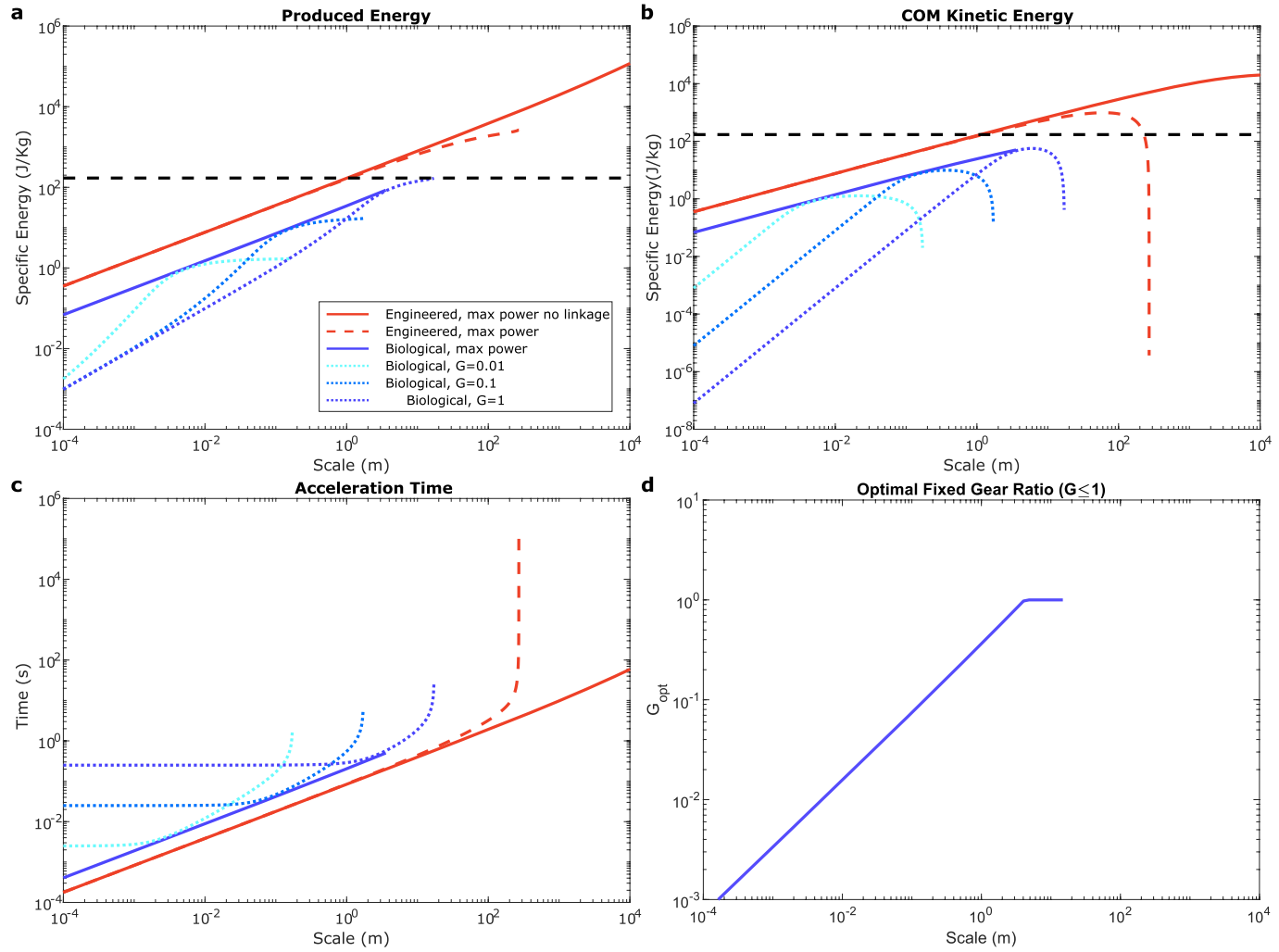

Extended Data Fig. 3 | Direct-actuated jumper simulations. a, The produced energy specific to the jumper mass. **b**, The centre-of-mass kinetic energy, specific to the jumper mass. **c**, The acceleration time. **d**, The optimal fixed reduction, *G*, producing the highest acceleration velocity for each jumper scale. The simulations are performed (i) for biological jumpers with fixed reductions of 0.01, 0.1, and 1 (dotted lines), and (ii) for biological jumpers (blue solid) and engineered jumpers (red solid: no linkage; red dotted: with linkage) using variable reduction to operate at maximum power. Each fixed reduction is only possible up to a limiting scale, where the motor force balances the body weight. Biological jumpers operating at full power are also limited in scale, as the motor runs out of stroke. Consequently, biological energy production is always limited by the motor energy (black dashed line). Finally, when operating at the optimal fixed or full-power variable reduction, the acceleration time scales with a 2/3 power of size, reflected in the same scaling in energy and gear reduction.

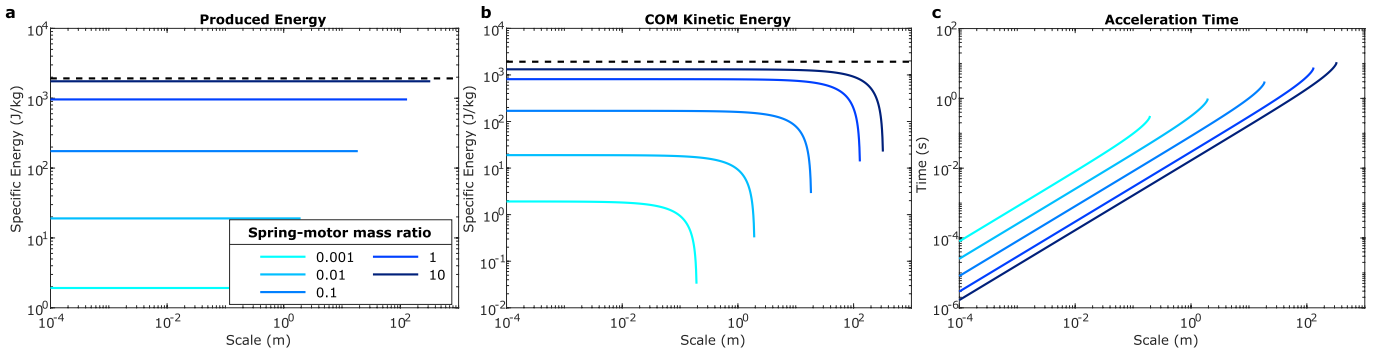

Extended Data Fig. 4 | Spring-actuated engineered jumper simulations. **a**, The produced energy specific to the jumper mass. **b**, The centre-of-mass kinetic energy, specific to the jumper mass. **c**, The acceleration time. The simulations are performed for spring mass ratios of ranging from 0.001–10. A lower mass ratio lowers the produced energy specific to the total mass and also imposes an upper bound on size, as smaller springs cannot match larger weight forces. The acceleration time scales nearly linearly with the size, and bigger springs create faster jumps.

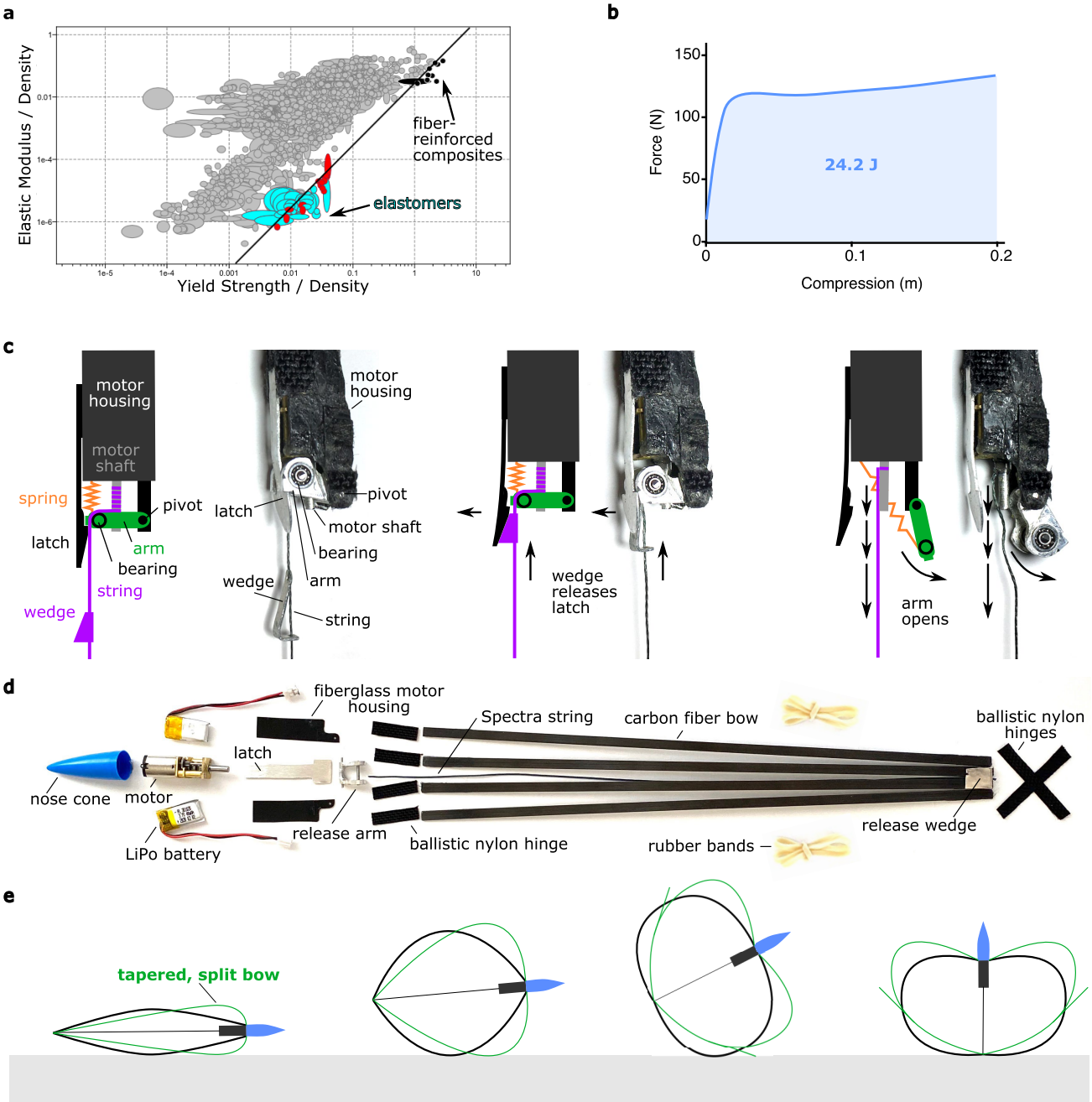

Extended Data Fig. 5 | Jumper design details. a, Ashby plot of materials with the largest material factor, or the square of yield strength over density. At low elastic moduli are elastomers, but these require a passive linkage to load in tension. At high elastic moduli are fibre-reinforced composites, which can act as stand-alone compression bow springs, but have lower specific energies than elastomers in tension. We therefore design a hybrid spring with elastomer in tension and carbon fibre in bending, replacing the passive linkage. **b**, Force–displacement plot of our hybrid linkage-spring, with total area under the curve (energy) shown (24.2 J). **c**, Schematic and pictures of the minimalistic release mechanism for unlatching. During winding of the string, the motor shaft turns, pulling the string over a shaft supported by bearings in the arm and compressing the hybrid spring-linkage. With further winding, a lever on the string eventually hits the latch, prying it open. The arm swings open, allowing the string to unspool from the shaft. **d**, Components of the jumper before assembly. **e**, Self-righting mechanism. Without a self-righting mechanism, the top-heavy jumper will roll nose-down during compression of the bow springs, given its mass distribution. However, if tapered and split bows are added between each pair of the main, non-tapered bow springs, the behaviour can be reversed. The taper in the bow near the nose creates a high radius of curvature during compression, contacting the ground and forcing the nose to roll upward. The split section continues this as the jumper nears completion of the righting behaviour.

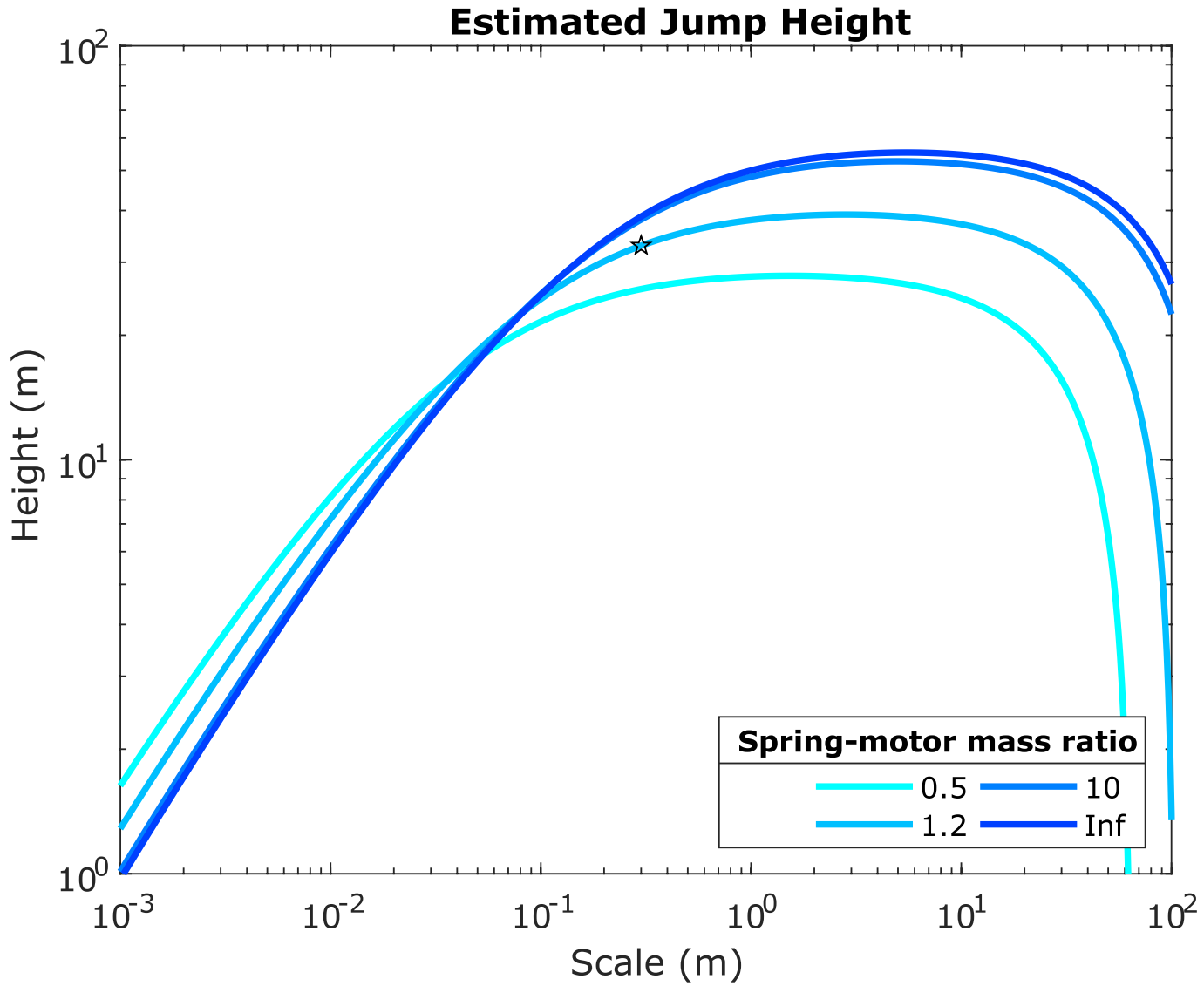

Extended Data Fig. 6 | Simulating the presented jumper across the spring–motor mass ratio and scale. Using the state-space model modified with the specifics of the presented jumper, we simulated jump height. We included both energy production and energy utilization. When the spring–motor mass ratio is increased to infinite, we see only a 17% increase in jump height (from 32.9 to 38.6 m). When the scale is increased by 10×, we find an increase of only 19% in jump height (from 32.9 to 39.1 m). The star denotes the presented jumper (0.3 m scale, 32.9 m jump height).

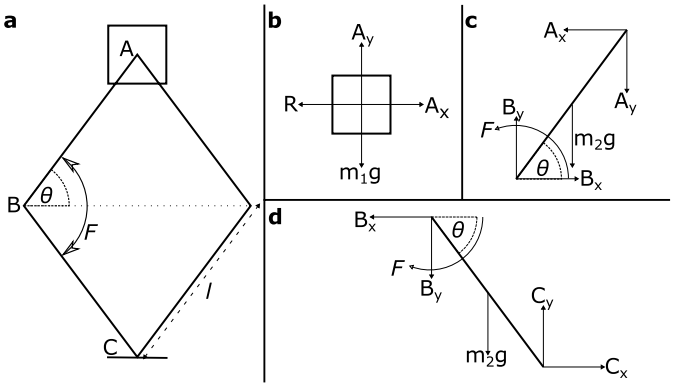

Extended Data Fig. 7 | Schematic of simplified jumper. a, Schematic of jumper used in Fig. 1a. **b**–**d**, Free-body diagrams of the body, top linkage, and bottom linkage, respectively.

Extended Data Table 1 | Biological jump data

Source	Scientific Name	Common Name	Length (m)	Velocity (m/s)	Time (s)	Mechanism Specific Energy (J/kg)	*in vacuo* Jump Height (m)
[53]	Salticidae	Jumping Spider	0.006	0.8	0.015	1.8	0.03
[54]	Acris gryllus	Southern cricket frog	0.034	2.3	0.033	15.3	0.26
[54]	*Pseudodacris crucifer*	spring peeper (frog)	0.038	2.4	0.036	17.6	0.30
[55]	*Schistocerca gregaria*	Desert locust, 1st instar	0.007	1.2	0.008	4.3	0.07
[54]	*Hyla squirella*	Squirrel tree frog	0.058	1.9	0.063	11.2	0.19
[54]	*Hyla cinerea*	American green tree frog	0.070	2.0	0.073	11.9	0.20
[56]	*Anolis carolinensis*	Green anole (lizard)	0.070	2.5	0.056	18.9	0.32
[54]	*Osteopilus septentrionalis*	Cuban tree frog	0.108	2.9	0.091	24.9	0.42
[57]	*Sciurus vulgaris*	Red squirrel	0.150	4.2	0.071	54.0	0.92
[54]	*Rana catesbiana*	American bullfrog	0.164	2.6	0.128	19.7	0.335
[58]	*Canis familiaris*	Dog	0.600	4.2	0.160	52.9	0.900
[59]	*Epiphyas postvittana*	Moth, light brown apple	0.010	1	0.011	3.0	0.051
[59]	*Xanthorhoe fluctuate*	Moth, garden carpet	0.013	1	0.016	3.0	0.051
[59]	*Crambus pascuella*	Moth, grass veneer	0.012	0.9	0.023	2.4	0.041
[60]	*Homo sapiens*	Human	1.000	3.1	0.360	29.4	0.500
[61]	*Psylliodes affinis*	Flea beetle	0.002	2.3	0.001	16.4	0.278
[62]	*Neophilaenus exclamationis*	Froghopper	0.004	4.2	0.001	52.9	0.900
[62]	*Philaenus spumarius*	Froghopper	0.006	4.7	0.001	66.3	1.127
[63]	*Athous haemorrhoidalis*	Click beetle	0.010	3.0	0.005	27.0	0.459
[62]	*Lepyronia coleoptrata*	Froghopper	0.007	4.6	0.002	63.5	1.080
[64]	*Collembola*	springtail	0.002	0.3	0.009	0.3	0.005
[61]	*Psylliodes dulcamarae*	Flea beetle	0.004	2.3	0.002	15.9	0.270
[65]	*Drosophila melanogaster*	Fruit fly larva	0.008	2.6	0.004	20.6	0.351
[63]	*Archaeognatha*	Bristletail	0.010	2.0	0.007	12.3	0.209
[62]	*Aphrophora alni*	Froghopper	0.010	3.4	0.003	34.7	0.590
[62]	*Cercopis vulnerata*	Froghopper	0.010	3.8	0.003	43.3	0.737
[55]	*Schistocerca gregaria*	Desert locust adult	0.041	2.6	0.023	19.8	0.337
[12]	*Galago senegalensis*	Lesser galago	0.160	6.7	0.095	134.4	2.286
[66]	*Zapus Trinotatus*	Jumping mouse	0.032	3.0	0.021	27.5	0.420
[67]	*Dipodomys ingens*	Kangaroo rat	0.090	2.8	0.064	23.5	0.400

Refs.[53–67].

Extended Data Table 2 | Engineered jumper data

Source	Name	Approx. Length (m)	Jump Height (m)	Energy (J)	Mechanism Mass (g)	Mechanism Specific Energy (J/kg)
-	Presented jumper	0.3	32	24.2	22.5	1075
[13]	Multi-Mo Bat	0.2	3.74	6.4	57	112
[15]	Locust-inspired	0.2	3.67	~1.3	12.1	~110
[16]	EPFL 7 g	0.1	1.4	0.154	3.6	43
[17]	EPFL Steerable	0.1	1.1	~0.16	7.6	~21
		Jumpers not using electromagnetic motors				
[46]	Sand flea	0.4	10	~500	~800	~625
[45]	Wheeled propane	0.3	7.5	~470	~1000	~470

Mechanism specific energy is calculated as the energy production divided by the mass of the mechanism (motor, spring and linkage). The '~' represents numbers estimated from source. Refs. [13,15–17,45,46].

Extended Data Table 3 | Jumper specifications

Component	Description	Mass (g)	Qty.	Total Mass (g)
Carbon rod	270 mm x 4.5 mm x 1.45 mm (ACP Composites)	2.75	4	11.0
Rubber bands	30.5 mm x 1.2 mm x 3.175 mm	0.0875	16	1.4
Motor	6V High-power Carbon Brush, 1.5A stall, 986.4:1 gear reduction, metal spur gears (Pololu)	10.1	1	10.1
Battery	3.7V LiPo (PKCELL) 105mAh	2.8	1	2.8
Release arm	Custom 7075 Al, with SS bearings and shafts (McMaster-Carr)	1.23	1	1.23
Nose cone	Injection molded model rocket cone	1.20	1	1.20
Motor housing	Custom fiberglass, 0.25 mm thick (ACP Composites)	0.97	1	0.97
Fabric hinge	Ballistic nylon (McMaster-Carr)	0.08	8	0.64
Latch	Custom 7075 Al (McMaster-Carr)	0.47	1	0.47
CA glue	Loctite 401	0.4	1	0.4
String	Spectra line, 300 N (PowerPro)	0.07	1	0.07
Wedge	Custom 7075 Al (McMaster-Carr)	0.05	1	0.09
TOTAL				**30.37**